Heriot-Watt University
Research Gateway

Wireless-powered CR-IoT with ambient backscattering

Citation for published version:
Sun, M, Ding, Y & Goussetis, G 2021, 'Wireless-powered CR-IoT with ambient backscattering: a new transmission mode', *IET Communications*, vol. 14, no. 22, pp. 4069-4074. https://doi.org/10.1049/iet-com.2019.1343

Digital Object Identifier (DOI):
10.1049/iet-com.2019.1343

Link:
Link to publication record in Heriot-Watt Research Portal

Document Version:
Peer reviewed version

Published In:
IET Communications

Publisher Rights Statement:
© 2021 IEEE. Personal use of this material is permitted. Permission from IEEE must be obtained for all other uses, in any current or future media, including reprinting/republishing this material for advertising or promotional purposes, creating new collective works, for resale or redistribution to servers or lists, or reuse of any copyrighted component of this work in other works.

General rights
Copyright for the publications made accessible via Heriot-Watt Research Portal is retained by the author(s) and / or other copyright owners and it is a condition of accessing these publications that users recognise and abide by the legal requirements associated with these rights.

Take down policy
Heriot-Watt University has made every reasonable effort to ensure that the content in Heriot-Watt Research Portal complies with UK legislation. If you believe that the public display of this file breaches copyright please contact open.access@hw.ac.uk providing details, and we will remove access to the work immediately and investigate your claim.

Download date: 18. May. 2025

Wireless-Powered CR-IoT With Ambient Backscattering: A New Transmission Mode

Mengwei Sun, Yuan Ding, George Goussetis, *Senior Member, IEEE*

In this paper, a new hybrid secondary transmitter (ST) mode is proposed for cognitive radio Internet of Things (CR-IoT) networks with energy harvesting (EH) and ambient backscatter (AmBack) communication capabilities. We firstly describe the proposed hybrid mode with wireless-powered ST. The ST, consisting of EH, Amback, and conventional active transmission modules, adapts itself under different primary user (PU) operation states, i.e. active or idle. The overall throughput of the secondary system is formulated and the system settings for achieving optimal performance are derived and validated through numerical simulations.

***Index Terms*—CR-IoT network, energy harvesting, ambient backscatter, optimal transmission mode.**

I. Introduction

THE Internet of Things (IoT), as one main pillar of the fifth generation (5G) communication eco-systems, envisions the wireless inter-connectivity among massive low-cost low-power devices [1] [2]. The explosive growth of IoT networks raises challenges facing the ever-scarce spectrum resources and long-term power maintenance such as battery replacement. To cope with the spectrum challenge, the cognitive radio (CR) technology provides a paradigm with opportunistic access strategies which can realize spectrum sharing and improve spectrum efficiency [3]. Therefore, an effectively enhanced IoT paradigm, namely cognitive radio Internet of Things (CR-IoT), was recently proposed [4] - [6]. To cope with the power supply challenge, the radio frequency (RF) energy harvesting (EH) technique is emerging as a promising candidate, which scavenges RF energy from ambient environment to support system operations [5]. One recent attempt of integrating EH and CR was presented in [6]. The authors proposed a harvest-then-transmit (HTT) CR model, which allows secondary users (SUs) to harvest energy from primary users (PUs) when PUs are active, and then use the captured energy to actively transmit data when the allocated frequency resources are released by PUs (i.e., PUs are idle). This proposed protocol can enhance the energy and spectrum efficiency simultaneously. However, the system performance is significantly limited when the PU experiences short idle period, within which the information of SUs can only be conveyed.

To deal with this problem, ambient backscatter (AmBack) has been introduced in CR-IoT networks [7] - [10]. With AmBack capacity, SU devices can create communication links to transmit data by modulating and reflecting an incident RF wave from PU sources [7] - [10]. Hybrid protocols combining AmBack and HTT can help SUs use the incident energy more efficiently and enhance the system performance limited by short PU idle period. In particular, [7] presented an AmBack-EH-transmit mode, in which an optimal time allocation strategy for these three phases to maximize the throughput was obtained. While [8] proposed two hybrid AmBack/HTT schemes to accommodate various channel conditions. It should be noted that in these works, two important aspects, i.e., energy consumption and spectrum efficiency, associated with AmBack modulation schemes were overlooked. The modulator of AmBack circuitry implements BPSK, QPSK and 16-PSK modulation using RF symbol switches [11]. Higher order modulation provides higher symbol rates at the cost of greater power consumption. For example, BPSK requires one single pole double throw (SPDT) switch, while QPSK doubles the throughput but requires three SPDT switches [11].

Otherwise, with a full-duplex antenna equipped at secondary transmitter (ST), simultaneous transmission and reception are allowed [12] - [14]. As RF signals can carry both energy and information at the same time according to [15] - [17], the information and power transfer can be performed simultaneously on the same incident signal at the ST node. In applying the above principles, we introduce a new hybrid HTT and AmBack mode to maximize the SUs system throughput. Compared with [7] and [8], the ST in our proposed model can work in both HTT and AmBack modes such that the information transmission duration can be fully extended. Compared with [9] and [10], the EH and AmBack operations can be realized in one device, which can help to reduce the network complexity. In addition, the power consumption and the effects to AmBack rate from AmBack modulation schemes are taken into consideration. The contributions are summarized as follows.

- We present a hybrid AmBack-HTT mode to exploit the advantages of both HTT and AmBack modes. During the period when PUs are busy, EH and AmBack are simultaneously processed at ST node. Specifically, the energy of the incident RF wave at the ST is used for two operations, EH and AmBack information transmission. The harvested energy enables the ST to operate in a self-sustainable manner and is split into two parts, one fraction is to activate SPDT switches for AmBack modulation, the other is stored into an energy storage for the active transmission of ST when PUs turn to be idle. The proposed hybrid AmBack-HTT mode takes fully into account the spectrum efficiency and power

M. W. Sun is with the University of Edinburgh, Edinburgh, EH9 3FG, UK (msun@ed.ac.uk)

Y. Ding and G. Goussetis are with the Heriot-Watt University, Edinburgh, EH14 4AS, UK (yuan.ding@hw.ac.uk; g.goussetis@hw.ac.uk)

This work was supported by the EPSRC EP/P025129/1 and the Carnegie Research Incentive Grant RIG008216.

consumption of the AmBack modulation.

- Then, an optimal power allocation mode which can maximize the SUs system throughput is studied by jointly investigating the optimal power allocation trade-off between the AmBack and HTT modes.
- Third, we present numerical results to show the proposed hybrid mode can significantly improve the throughput of the SUs' communication.

The paper is organized as follows. In Section II, we presented the designed hybrid AmBack-HTT mode and formulate the optimization problem. The mathematical derivations of the optimal power allocation scheme are provided in Section III. In Section IV and V, numerical results and conclusions are provided respectively.

II. System Model

In this section, we introduce the proposed hybrid AmBack-HTT mode in a CR-IoT network, as shown in Fig. 1(a). Denote the duration of the PU busy and idle periods as μT and $(1-\mu)T$ respectively. When the PU is busy, i.e., Phase I, the EH and AmBack transmission are processed simultaneously at the ST node. Once the PU turns to be idle, i.e., Phase II, the stored energy during Phase I is released for active transmission.

The work process of all the modules at ST node is shown in Fig. 1(b). The ST has two major operations, EH and information transmission. A full-duplex tag and a full-duplex antenna are equipped into the ST as the feasibility to allow simultaneous transmission and reception [13] [14]. As RF signals can carry both energy and information simultaneously [15] - [17], the information and power transfer are performed at the same time. Specifically, when the PU is detected to be busy, the incident power at ST node from PU is denoted as P_R. Part of the the incident energy is harvested relying on the energy harvest device and the rest signal is modulated by the micro-controller and scattered to the secondary receiver (SR). The harvested energy is split into two fractions. One is used for activating the switches of the SPDT device to modulate data packets using the micro-controller. Note, in order to avoid the detrimental interference to the weak backscatter link caused by the ambient signals, the backscatter links are commonly frequency shifted [19] [20]. The other is stored into the energy storage for active transmission when the PU becomes idle. The power allocated to SPDT switches, energy storage and signal backscatter are αP_R, βP_R and $(1-\alpha-\beta)P_R$, respectively, where $\alpha+\beta \in [0,1]$.

The total system throughput R consists of achievable throughputs during two phases and is thus given by [10],

$$R(\alpha,\beta) = R_1(\alpha,\beta) + R_2(\alpha,\beta). \tag{1}$$

The Shannon capacity is derived based on the assumption that the input signal follows a Gaussian distribution, while in AmBack transmission, this assumption may be invalid which leads to a performance gap between the channel capacity of AmBack and Shannon capacity. In this work, $\zeta(0<\zeta<1)$ is used to represent this performance gap [18]. Therefore, the throughput in Phase I and Phase II can be expressed as:

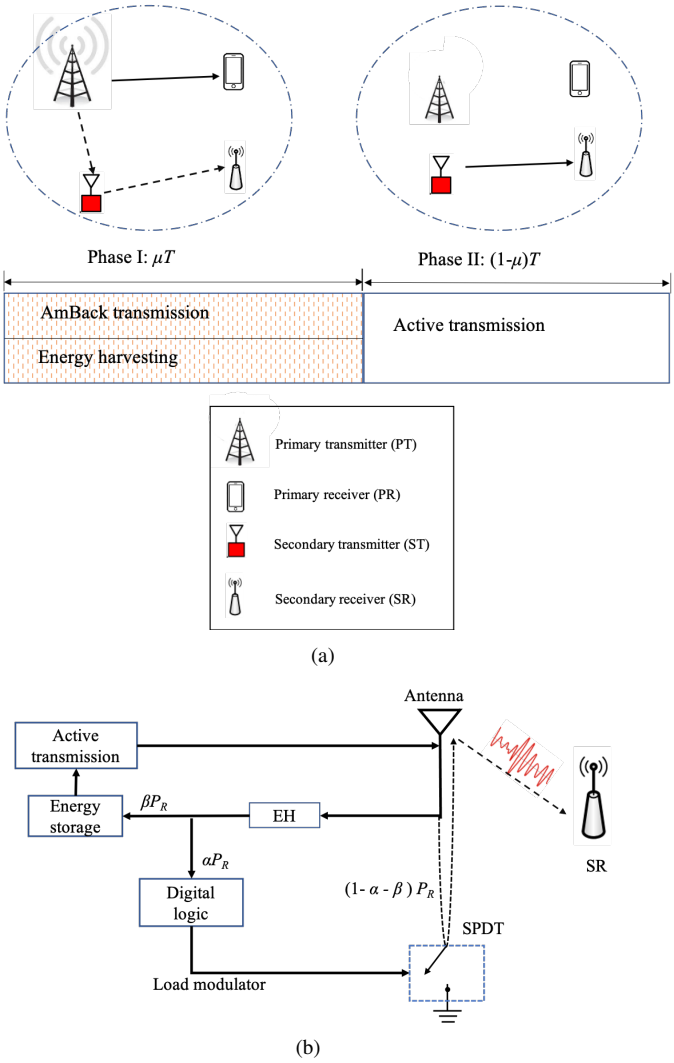

Fig. 1: (a) System model and time scheduling structure. (b) Block diagram of different modules at the ST node.

$$R_1(\alpha,\beta) = \mu B\left[1+\zeta\frac{P_1}{P_0}\right], \tag{2}$$

$$R_2(\alpha,\beta) = (1-\mu)W\left[1+\frac{P_2}{P_0}\right]. \tag{3}$$

where the available bandwidth in Phase I is denoted as B. The bandwidth B is determined by the available switching rate for SPDT and is calculated as $B = \eta\frac{\lambda\alpha P_R}{\epsilon}$. Here, λ denotes the EH efficiency and $\lambda\alpha P_R$ is the harvested energy used for SPDT switch. ϵ represents the energy cost for each switching operation [5]. Therefore, the symbol rate can be calculated by $\frac{\lambda\alpha P_R}{\epsilon}$. η denotes the spectrum efficiency for different modulation scheme and $\eta=1$ when the modulation scheme is set to be BPSK [11]. The received signal to noise ratio (SNR) at the SR is calculated as P_1/P_0, where $P_1 = \xi(1-\alpha-\beta)P_R$, and $\xi(0<\xi<1)$ represents the transmission efficiency. P_0 represents the noise power. Note, conventional AmBack communication links are limited to amplitude and

frequency shifted keying modulation schemes, while the recent developments have shown that more advanced backscatter modulation schemes, like high-order QAM [19], CSS [20], and OFDM [21] are achievable. The link capacity is highly dependent on the selected backscattering modulation schemes and the support tag hardware architecture. This paper is not dedicated to a specific backscattering modulation scheme. Instead, it aims to reveal the boundary of the achievable capacity of the backscattering links and the entire network. W and P_2 represent the bandwidth and transmitted power for the active transmission during Phase II. $P_2 = \xi\frac{\mu\lambda\beta P_R}{1-\mu}$. The transmission efficiency ξ of the active transmission is assumed to be identical to the AmBack transmission, which accounts for the associated antenna loss and circuit power consumption. Based on the above, we can rewrite (1) as,

$$\begin{aligned} R(\alpha,\beta) =& \mu\frac{\eta\lambda\alpha P_R}{\epsilon}\log_2\left[1+\zeta\frac{\xi(1-\alpha-\beta)P_R}{P_0}\right], \\ &+(1-\mu)W\log_2\left[1+\frac{\xi\mu\lambda\beta P_R}{(1-\mu)P_0}\right]. \end{aligned} \tag{4}$$

Our target is to seek optimal α and β which maximize the throughput for SUs, i.e.,

$$(\alpha^\dagger,\beta^\dagger) = \max_{\alpha,\beta} R(\alpha,\beta), \tag{5}$$

$$\text{s.t. } \alpha+\beta\le 1. \tag{6}$$

III. Optimal Power Allocation Strategy

In this section, we firstly derive the marginal optimization of α and β respectively. Then, the joint global optimization of (α,β) is achieved.

A. Marginal optimization for α

The first and second partial derivatives of $R(\alpha,\beta)$ with respect to α can be derived as (7) and (8) respectively.

$$\begin{aligned} D_1(\alpha,\beta) =& \frac{\partial R(\alpha,\beta)}{\partial\alpha} = \frac{\mu\eta\lambda P_R}{\epsilon}\times \\ &\left\{\log_2\left[1+\frac{\zeta\xi(1-\alpha-\beta)P_R}{P_0}\right]-\frac{\zeta\xi P_R\alpha}{[\zeta\xi(1-\alpha-\beta)P_R+P_0]\ln 2}\right\}. \end{aligned} \tag{7}$$

$$\begin{aligned} U_{1,1}(\alpha,\beta) =& \frac{\partial D_1(\alpha,\beta)}{\partial\alpha}, \\ =& -\frac{\zeta\xi\mu\eta\lambda P_R^2\left[2P_0+\zeta\xi(2-\alpha-2\beta)P_R\right]}{\epsilon\left[\zeta\xi(1-\alpha-\beta)P_R+P_0\right]^2\ln 2}<0. \end{aligned} \tag{8}$$

Obviously,

$$D_1|_{\alpha=0} = \frac{\mu\eta\lambda P_R}{\epsilon}\log_2\left[1+\frac{\zeta\xi(1-\beta)P_R}{P_0}\right]>0, \tag{9}$$

$$D_1|_{\alpha=1-\beta} = -\frac{\mu\eta\lambda P_R}{\epsilon}\frac{\zeta\xi P_R(1-\beta)}{P_0\ln 2}<0. \tag{10}$$

(9) and (10) indicates that $R(\alpha,\beta)$ increases versus α is small but decreases when α approaches $1-\beta$. Hence, there is an optimal α within the interval $[0,1-\beta]$ corresponding to the maximum $R(\alpha,\beta)$ for each fixed β. (8) indicates that $D_1(\alpha,\beta)$ is decreasing versus α, which further implies $R(\alpha,\beta)$ is concave with respect to α. Therefore, we can have:

Remark 1: The marginal optimal α^* uniquely exists for each fixed β.

B. Marginal optimization for β

The first and second partial derivatives of $R(\alpha,\beta)$ with respect to β are derived as followings:

$$\begin{aligned} D_2(\alpha,\beta) =& \frac{\partial R(\alpha,\beta)}{\partial\beta} = \frac{\xi\mu\lambda P_R}{\ln 2}\times \\ &\left\{-\frac{\eta\zeta\alpha P_R}{\epsilon\left[\zeta\xi(1-\alpha-\beta)P_R+P_0\right]}+\frac{(1-\mu)W}{\xi\mu\lambda\beta P_R+(1-\mu)P_0}\right\}. \end{aligned} \tag{11}$$

$$\begin{aligned} U_{2,2}(\alpha,\beta) =& \frac{\partial D_2(\alpha,\beta)}{\partial\beta}, \\ =& -\frac{\xi^2\mu\lambda P_R^2}{\ln 2}\left\{\frac{\eta\zeta\alpha P_R}{\epsilon\left[\zeta\xi(1-\alpha-\beta)P_R+P_0\right]^2}\right. \\ &\left.+\frac{(1-\mu)W}{\left[\xi\mu\lambda\beta P_R+(1-\mu)P_0\right]^2}\right\}<0. \end{aligned} \tag{12}$$

Then,

$$D_2|_{\beta=0} = \frac{\xi\mu\lambda P_R}{\ln 2}\left\{-\frac{\eta\zeta\alpha P_R}{\epsilon\left[\zeta\xi(1-\alpha)P_R+P_0\right]}+\frac{W}{P_0}\right\}, \tag{13}$$

$$D_2|_{\beta=1-\alpha} = \frac{\xi\mu\lambda P_R}{\ln 2}\left\{-\frac{\eta\zeta\alpha P_R}{\epsilon P_0}+\frac{(1-\mu)W}{\xi\mu\lambda(1-\alpha)P_R+(1-\mu)P_0}\right\}. \tag{14}$$

(12) indicates that $D_2(\alpha,\beta)$ is decreasing with respect to $\beta\in[0,1-\alpha]$. Considering the values of D_2 when $\beta=0$ and $\beta=1-\alpha$ as shown in (13) and (14) respectively, the conclusions can be drawn as $D_2|_{\beta=0}\underset{\mathcal{H}_1}{\overset{\mathcal{H}_0}{\lessgtr}}0$, where $\mathcal{H}_0: W<T_1$, $\mathcal{H}_1: W>T_1$ and $T_1\triangleq\frac{\eta\zeta\alpha P_R P_0}{\zeta\epsilon\left[\xi(1-\alpha)P_R+P_0\right]}$. Similarly, $D_2|_{\beta=1-\alpha}\underset{\mathcal{G}_1}{\overset{\mathcal{G}_0}{\lessgtr}}0$, where $\mathcal{G}_0: W<T_2$, $\mathcal{G}_1: W>T_2$ and $T_2\triangleq\frac{\eta\zeta\alpha P_R\left[\xi\mu\lambda(1-\alpha)P_R+(1-\mu)P_0\right]}{\epsilon P_0(1-\mu)}$. Furthermore, T_2 is constantly greater than T_1, see (15).

$$\begin{aligned} T_2 =& \frac{\eta\zeta\alpha P_R P_0}{\epsilon P_0}+\frac{\eta\zeta\alpha P_R^2\xi\mu\lambda(1-\alpha)}{\epsilon P_0(1-\mu)}, \\ \ge& \frac{\eta\zeta\alpha P_R P_0}{\epsilon\left[\xi(1-\alpha)P_R+P_0\right]}+\frac{\eta\zeta\alpha P_R^2\xi\mu\lambda(1-\alpha)}{\epsilon P_0(1-\mu)}, \\ =& T_1+\frac{\eta\zeta\alpha P_R^2\xi\mu\lambda(1-\alpha)}{\epsilon P_0(1-\mu)}\ge T_1. \end{aligned} \tag{15}$$

Then, the following *Remarks* can be drawn,

- *Remark 2*: Case 1, if the bandwidth for active ST transmission $W\in(0,T_1)$, $R(\alpha,\beta)$ is monotone decreasing with respect to β, and thus, the optimal value for β is $\beta^*=0$.
- *Remark 3*: Case 2, if $W\in(T_2,\infty)$, $R(\alpha,\beta)$ is monotone increasing, and the optimal value for β is $\beta^*=1$.
- *Remark 4*: Case 3, if $W\in[T_1,T_2]$, an optimal $\beta^*\in[0,1-\alpha]$ uniquely exists for a fixed α.

The second mixed partial derivative with respect to (α,β) can be further derived as,

$$\begin{aligned} U_{1,2}(\alpha,\beta) =& \frac{\partial R^2(\alpha,\beta)}{\partial\alpha\partial\beta} = \frac{\partial D_1(\alpha,\beta)}{\partial\beta} \\ =& -\frac{\mu\eta\lambda\zeta\xi P_R^2}{\epsilon}\frac{\zeta\xi(1-\beta)P_R+P_0}{\left[\zeta\xi(1-\alpha-\beta)P_R+P_0\right]^2\ln 2}<0. \end{aligned} \tag{16}$$

Then, the conclusion is achieved as D_1 is monotonically decreasing with respect to α. Therefore, under Case 1-3, the optimal β^* decreases within the increasing given value of α.

C. Global optimization for (α,β)

Under Case 1, the global optimal $\beta^\dagger = \beta^* = 0$, which means all the incident energy should used in the passive transmission stage, including αP_R for AmBack modulation, and $(1-\alpha)P_R$ for AmBack backscattering. The corresponding optimal α can be obtained via $D_1(\alpha^\dagger, 0) = 0$.

Under Case 2, the optimal allocation strategy is $(\alpha^\dagger,\beta^\dagger) = (0,1)$, i.e., all the incident energy is harvested and stored for the active transmission when the PU is idle.

Under Case 3, the stationary point of $R(\alpha,\beta)$ can be obtained by solving $D_1(\alpha,\beta) = D_2(\alpha,\beta) = 0$, saying $(\alpha^\ddagger,\beta^\ddagger)$. The discriminant of $R(\alpha,\beta)$ at this stationary point is,

$$\triangle(\alpha^\ddagger,\beta^\ddagger) = U_{1,1}(\alpha^\ddagger,\beta^\ddagger)U_{2,2}(\alpha^\ddagger,\beta^\ddagger) - U^2_{1,2}(\alpha^\ddagger,\beta^\ddagger). \quad (17)$$

Here, the second partial derivatives $U_{11}(\alpha,\beta)$ and $U_{22}(\alpha,\beta)$ have been derived in (8) and (10) which are always negative.

- If $\triangle < 0$, $(\alpha^\ddagger,\beta^\ddagger)$ is a saddle point.
- If $\triangle > 0$, $(\alpha^\ddagger,\beta^\ddagger)$ is either a maximum or a minimum point, depending on:
  - ◇ If $U_{1,1}(\alpha^\ddagger,\beta^\ddagger) < 0$ and $U_{2,2}(\alpha^\ddagger,\beta^\ddagger) < 0$, $(\alpha^\ddagger,\beta^\ddagger)$ is a maximum point, i.e., the target optimal point in (3).
  - ◇ If $U_{1,1}(\alpha^\ddagger,\beta^\ddagger) > 0$ and $U_{2,2}(\alpha^\ddagger,\beta^\ddagger) > 0$, $(\alpha^\ddagger,\beta^\ddagger)$ is a minimum point.

IV. Numerical Results and Performance Evaluation

For simulations in this section, the values of system parameters used are shown in Table I following some practical values used in [7], [11] and [18]. It should be noted that the analyses and conclusions achieved in our paper are not affected by these parameters settings as it gives the optimal power allocations rates for energy harvesting and AmBack transmission.

TABLE I: Summay of System Parameters Used

Notation	Definition	Value
P_R	Received Power at ST from PU	10 dBm
λ	Efficiency of EH	0.4
ζ	Performance gap of AmBack	0.5
ξ	Transmission efficiency	0.8
η	Spectrum efficiency of BPSK modulation	1
ϵ	Energy cost for each symbol switching	25μJ/s
μ	Time fraction of active state for PU	0.7
P_0	Noise power	−10dBm

A. Remarks Validations

Fig. 2(a) shows the first partial derivative $D_1(\alpha,\beta)$ surface with the zero-flat, the correspond intersection line shown in Fig. 2(b) indicates that the marginal optimal α^* is uniquely existing for a fix β, validating the *Remark 1*. Then, We verify the *Remarks 2-4* (Cases 1-3) with different W. Case 1, the throughput of secondary system $R(\alpha,\beta)$ illustrated in Fig. 3(a) is decreasing with greater β, which indicates that the

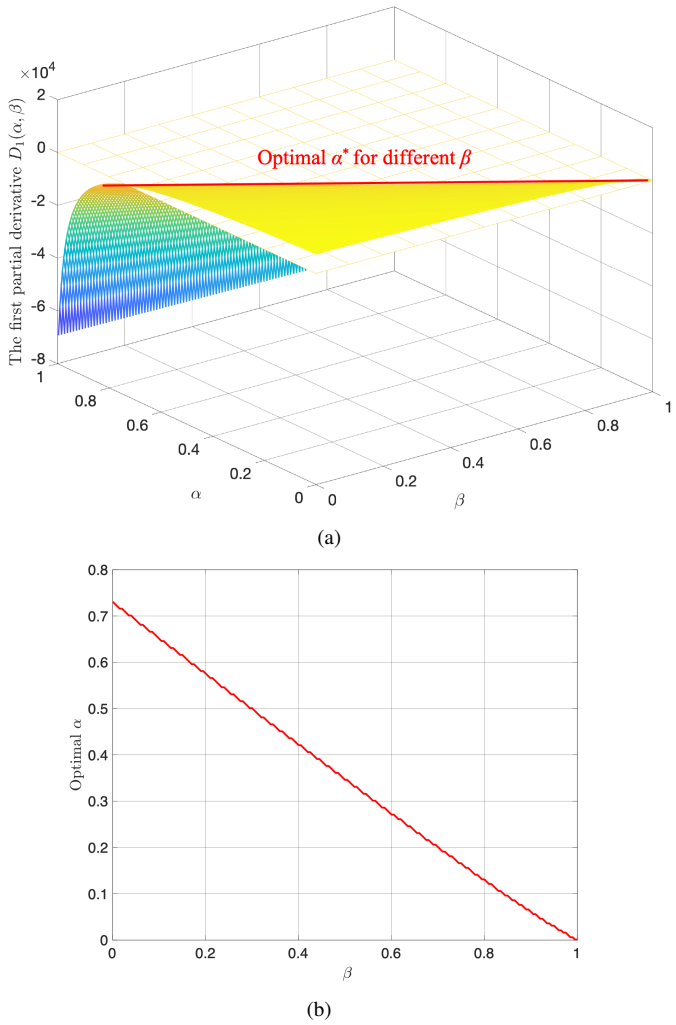

Fig. 2: (a) The first partial derivative of throughput with respect to α. (b) Optimal α allocated with the increasing chosen β.

marginal optimal $\beta^* = 0$. Case 2, the $R(\alpha,\beta)$ shown in Fig. 3(b) is monotone increasing with β which indicates the marginal optimal $\beta^* = 1$. Case 3, $D_2(\alpha,\beta)$ and the intersection line of $D_2(\alpha,\beta)$ with the zero-flat are provided in Fig. 4(a) and Fig. 4(b) respectively, which can refer to the marginal optimal β^* corresponding to different chosen α.

B. Throughput of Secondary System Evaluation

We firstly evaluate the optimal $(\alpha^\ddagger,\beta^\ddagger)$ with different AWGN power under Case 1. As the conclusion derived in Section III.C, the global optimal $\beta^\ddagger = 0$ under Case I, and the simulation results of $\alpha^\ddagger$ are shown in Fig.5. In noisier channel, the throughput decreases as we expect, and more incident energy should be backscattered with reduced symbol rates.

Then, the stationary points and the corresponding discriminant values under Case 3 are achieved. We vary the PU active period μ and observe its impact to the transmission policy as well as the throughput performance of the secondary system. As shown in Fig. 6(a), the discriminant value $\triangle$ is constant greater than zero, combining with the conclusion of

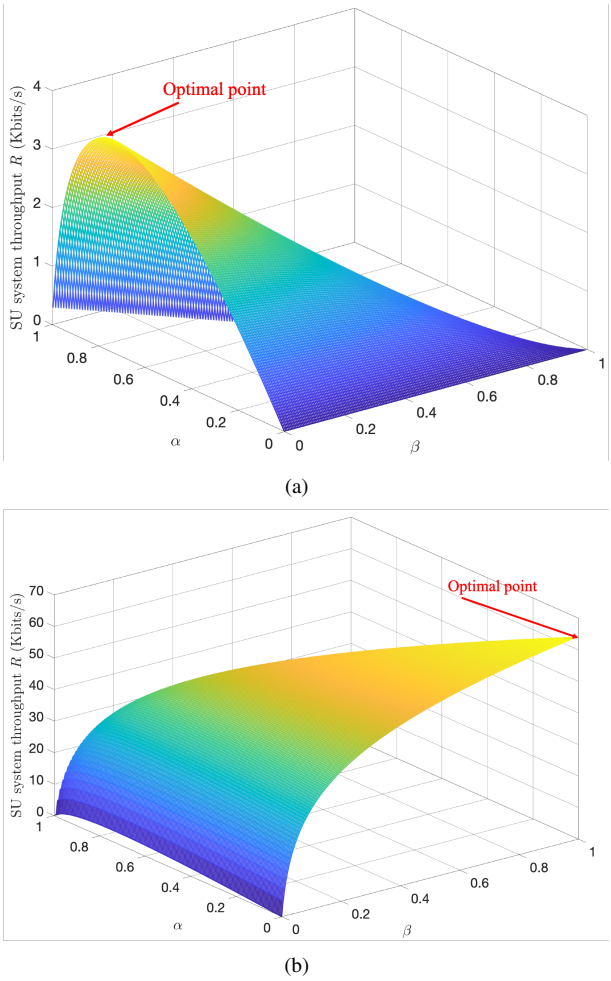

Fig. 3: System throughput under different W values. (a) Case 1, $W \in (0, T_1)$. (b) Case 2, $W \in (T_2, \infty)$.

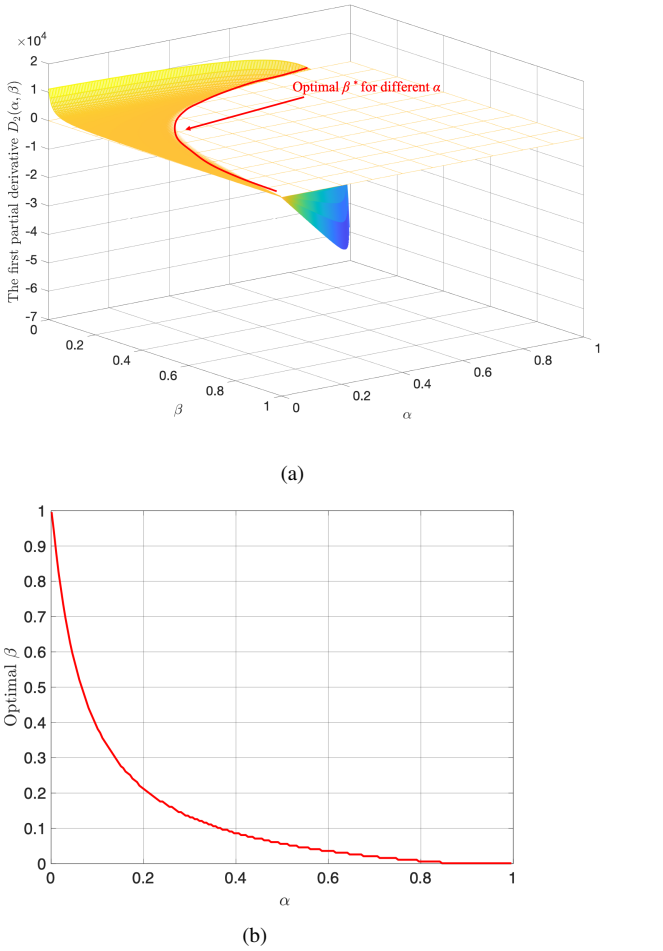

Fig. 4: (a) The first partial derivative of $R(\alpha,\beta)$ with respect to β under Case 3. (b) Optimal β allocated with the increasing chosen α under Case 3.

(10) and (12), we can have that the stationary points shown in Fig. 6(b) are the optimal mode. From Fig. 6(b), we can have that within the increasing $\mu^\dagger$, the optimal $\beta^\dagger$ is monotone decreasing while the optimal α and $1-\beta^\dagger-\alpha^\dagger$ is monotone increasing. In other words, less power should be stored for the active transmission, while more power should be allocated for both switching the SPDT and backscatter transmission.

Finally, we show numerical results through performing simulation experiments comparing with HTT mode [8] and all-backscattering mode, to demonstrate the performance enhancement of the proposed solution. From the simulation results shown in Fig. 6, we can see clearly that, the proposed solution always achieves the best performance compared with other two modes. And under Case 1, the proposed optimal mode becomes the all-backscattering mode. Otherwise, under Case 2, the proposed optimal mode is equivalent to the HTT mode.

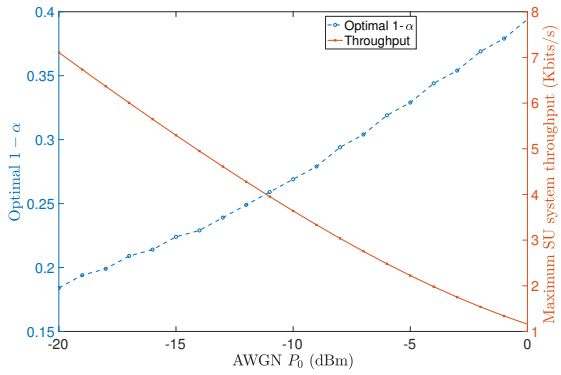

Fig. 5: Optimal $1-\alpha^\dagger$ with different AWGN power under Case 1.

V. Conclusions

In this paper, we proposed a hybrid transmitter mode by integrating EH and AmBack capabilities with wireless-powered CR-IoT networks. We have also investigated the throughput performance of the secondary system by formulating the optimization problems for the ST and obtaining the optimal power allocation and transmission scheme. Through numerical results, we have demonstrated that with the proposed transmission mode, the secondary system always achieves the best throughput performance compared with other reported works.

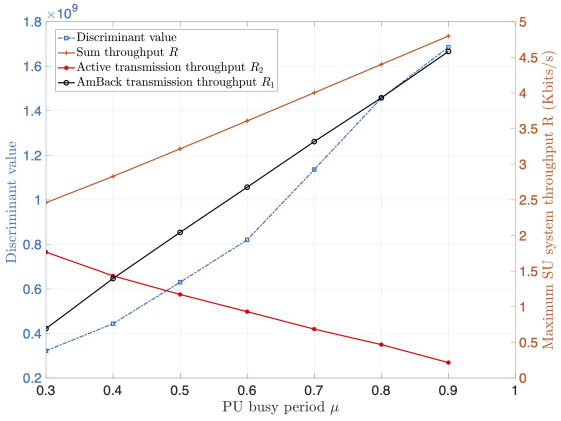

(a)

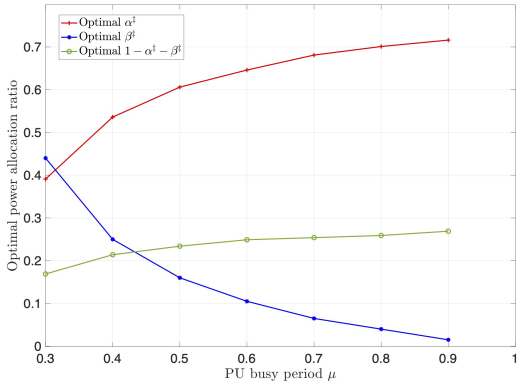

(b)

Fig. 6: Maximum throughput and optimal allocation mode under Case 3.

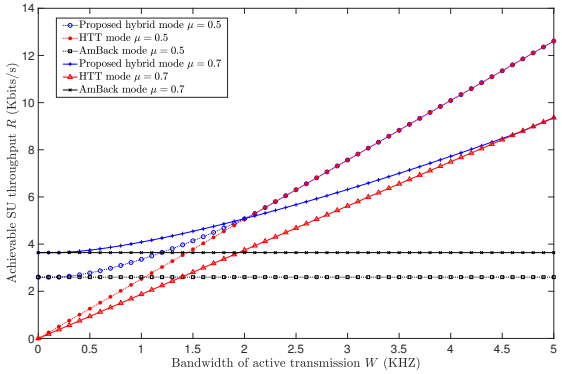

Fig. 7: Comparison of system throughput performance

References

[1] A. Al-Fuqaha, M. Guizani, M. Mohammadi, M. Aledhari, and M. Ayyash, "Internet of Things: A survey on enabling technologies, protocols, and applications," *IEEE Commum Surv Tut.*, vol. 17, no. 4, pp. 2347-2376, Jun. 2015.

[2] X. Kang, Y. -C. Liang, and J. Yang, "Riding on the Primary: A new spectrum sharing paradigm for wireless-powered IoT devices,"" *IEEE Internet Things J.*, vol. 1, no. 2, pp. 129-143, Mar. 2014.

[3] Federal Communication Commission, Spectrum Policy Task Force Report, ET Docket no.02-155, Nov. 2002.

[4] T. Li, J. Yuan, and M. Torlak, "Network throughput optimization for random access narrowband cognitive radio internet of things (NB-CR-IoT)," *IEEE Signal Process. Mag.*, vol. 5, no. 3, pp. 1436-1448, Jan. 2018.

[5] N. V. Huynh, D. T, Hoang, X. Lu, D. Niyato, P. Wang, and D. I. Kim, "Ambient backscatter communications: A contemporary survey," *IEEE Commum Surv Tut.*, vol. 20, no. 4, pp. 2899-2922, May 2018.

[6] S. Bi, Y. Zeng, and R. Zhang, "Wireless powered communication networks: An overview," *IEEE Wireless Commun.*, vol. 23, no. 4, pp. 1018, Apr. 2016.

[7] D. T. Hoang, D. Niyato, P. Wang, D. I. Kim, and Z. Han, "Ambient backscatter: A new approach to improve network performance for RF-powered cognitive radio networks," *IEEE Trans. Commun.*, vol. 65, no. 9, pp. 3659-3674, Jun 2017.

[8] D. Li, W. Peng, and Y. -C. Liang, "Hybrid ambient backscatter communication systems with harvest-then-transmit protocols," *IEEE Access*, vol. 6, pp. 45288-345298, Aug. 2018.

[9] B. Lyu, H. Guo, Z. Yang and G. Gui, "Throughput maximization for hybrid backscatter assisted cognitive wireless powered radio networks," *IEEE Internet Things J.*, vol. 5, no. 3, pp. 2015-2024, Jun. 2018.

[10] B. Lyu, Z. Yang, F. Tian and G. Gui, "Energy-efficient resource allocation for wireless-powered backscatter communication networks," in *Proceedings of the 2018 IEEE International Conference on Communication Systems (ICCS)*, Chengdu, China, 2018, pp. 72-77.

[11] D. Bharadia, K. Joshi, M. Kotaru, and S. Katti, "BackFi: High throughput WiFi backscatter," *ACM SIGCOMM Computer Communication Review - SIGCOMM'15*, vol. 45, no. 4, pp. 283-296, Oct. 2015.

[12] D. Bharadia, E. McMilin, and S. Katti, "Full duplex radios," in *Proc. ACM SIGCOMM*, 2013, pp. 375386.

[13] W. Liu, K. Huang, X. Zhou, and S. Durrani, "Full-duplex backscatter interference networks based on time-hopping spread spectrum," *IEEE Transactions on Wireless Communications*, vol. 16, no. 7, pp. 4361-4377, Jul. 2017.

[14] Liu, W., Huang, K., Zhou, X. et al. "Next generation backscatter communication: systems, techniques, and applications," *J. Wireless Com. Network*, no. 69, 2019.

[15] X. Liu, Y. Gao and F. Hu, "Optimal time scheduling scheme for wireless powered ambient backscatter communications in IoT networks," *IEEE Internet Things J.*, vol. 6, no. 2, pp. 2264-2272, Apr. 2019.

[16] F. Jameel , T. Ristaniemi , I. Khan and B. M. Lee, "Simultaneous harvest-and-transmit ambient backscatter communications under Rayleigh fading," *EURASIP J Wirel Commun Netw.* 166(2019), Jun. 2019.

[17] T. L. N. Nguyen, J.-Y. Kim, and Y. Shin, "Ambient Backscattering-Enabled SWIPT Relaying System with a Nonlinear Energy Harvesting Model," *Sensors (Basel, Switzerland)*, vol. 20, no. 16, 4534, Aug. 2020.

[18] Y. Ye, L. Shi, X. Chu and G. Lu, "Throughput fairness guarantee in wireless powered backscatter communications with HTT," *IEEE Wireless Communications Letters*, accepted, 2020.

[19] Y. Peng, L. F. Shangguan, Y. Hu et al. "PLoRa: a passive long-range data network from ambient LoRa transmissions", in *Proceedings of the 2018 Conference of the ACM Special Interest Group on Data Communication - SIGCOMM 18*, pp. 147160, Aug. 2018.

[20] B. Kellogg, V. Talla, J. R. Smith, and S. Gollakot, "Passive WI-FI: Bringing low power to Wi-Fi transmissions," *GetMobile Mob. Comput. Commun.*, vol. 20, no. 3, pp. 3841, Jan. 2017.

[21] Y. Ding, G. Goussetis, R. Correia et al., "Signal modulation schemes in backscatter communications", *Backscattering and RF Sensing for Future Wireless Communication*, in press.